Shape Reconstruction of Dielectric and Conducting Objects using Linear Sampling Method and Limitations

Mallikarjun Erramshetty
Department of Electronics and Communication Engineering
National Institute of Technology Goa, India
Email: emallikarjuna@nitgoa.ac.in

Amitabha Bhattacharya
Department of Electronics and Electrical Communication Engineering
Indian Institute of Technology Kharagpur, India
Email:amitabha@ece.iitkgp.ac.in

***Abstract*—This paper aims to investigate the behaviour of linear inverse method, linear sampling method (LSM), to estimate geometric properties of dielectric/ conducting objects. LSM is a simple, reliable linear inverse algorithm and uses multiview multistatic scattered field data measured around target objects. Despite its simplicity and computational effectiveness, LSM fails to detect targets support at certain frequencies (eigenvalues). The present work focusses on the occurrence of eigenvalues with respect to the object geometric properties. All these analyses are done by considering the numerical examples of synthetic data as well as experimental data provided by Institute of Fresnel.**

***Keywords*—Conductors, detection, dielectrics, linear sampling method.**

I. Introduction

Non-destruction evaluation of unknown objects has many applications in the field of military, civil, industrial, and so on. [1]. LSM is a simple, reliable and effective tool to estimate the shapes and locations of the dielectric and/or metallic objects through multi-view-multi-static measured scattered fields [2] . The method has a wide range of applications in 2-D and 3-D configurations in the presence of isotropic as well as anisotropic scatterers [3], [4]. In addition, the method has very low computational time. This method has been extensively studied from mathematical point of view, still issues such as limitations of LSM and how to use it in practice, have not been well addressed. In our recent work [5], we have shown that the LSM fails to detect the target points at certain frequencies due to the occurrence of eigenvalues. The analysis is carried out by considering the circular geometry and the results are concluded. In extension to the works reported in [5], the present work aims to find out weather the LSM possess similar behaviour for non-circular objects, if yes, what could be the effect on eigenvalues. The analysis are carried out by considering the numerical examples of synthetic data as well as experimental data. The rest of the paper is organized as follows. A Brief note about LSM and numerical results are discussed in Section II, The results are concluded in Section III.

II. Linear Sampling Method

Let us consider the objects under investigation are illuminated by an incident field from a direction φ_i and the resulted scattered fields be measured at a far-field distance $\underline{r}$. According to LSM, the targets support is estimated through the solution of far-field equation [2],

$$F[\xi] = \int_0^{2\pi} E^{scat}(\underline{r}, \varphi_i)\xi(\underline{z}_t, \varphi_i)d\varphi_i = G(\underline{r}, \underline{z}_t) \quad (1)$$

where G is a point source, $\underline{z}_t = (x,\, y)$ is a sampling point that spans the considered investigation area, and ξ is an unknown complex function that weights the scattered fields due to scattering objects in such a way that the resultant field look like the field radiated from the point source located at $\underline{z}_t$. F is a compact far-field operator [2]. $F : L^2(\Gamma) \rightarrow L^2(\Gamma)$.

To estimate the target' support, Eq. 1 is to be solved for each $\underline{z}_t$. According to the principle of LSM, the solution in the energy form $\|\xi(\underline{z}_t)\|^2$ is bounded if $\underline{z}_t$ belongs to the scatterer support and unbounded elsewhere. Here, $\|\cdot\|$ is the standard L^2-norm. Hence, Eq. 1 is ill-posed [6] and requires regularization for a stable solution. While referring to [2] for mathematical details, the final form of regularized solution based on the Singular Value Decomposition (SVD) technique [1] can be written as

$$\|\boldsymbol{\xi}(\underline{z}_t)\|^2 = \sum_{n=1}^{N} \left(\frac{\lambda_n}{\lambda_n^2 + \alpha}\right)^2 |\boldsymbol{f} \cdot \boldsymbol{\mu}_n|^2 \quad (2)$$

where λ_n and $\boldsymbol{\mu}_n$ are singular-values and left-singular-vector of F, respectively. $\boldsymbol{\xi}$ is the vector of unknowns, vector $\boldsymbol{f}$ is the far-field pattern radiated by the point source located at $\underline{z}_t$, N is the total number of non-zero singular values, and α is a regularization parameter. Therefore, the support of the scatterer is found by plotting $\|\boldsymbol{\xi}(\underline{z}_t)\|^2$ over the investigating domain. Parameter α is estimated using physics-based criteria as reported in [7], which does not require knowledge about noise level present in the measured data.

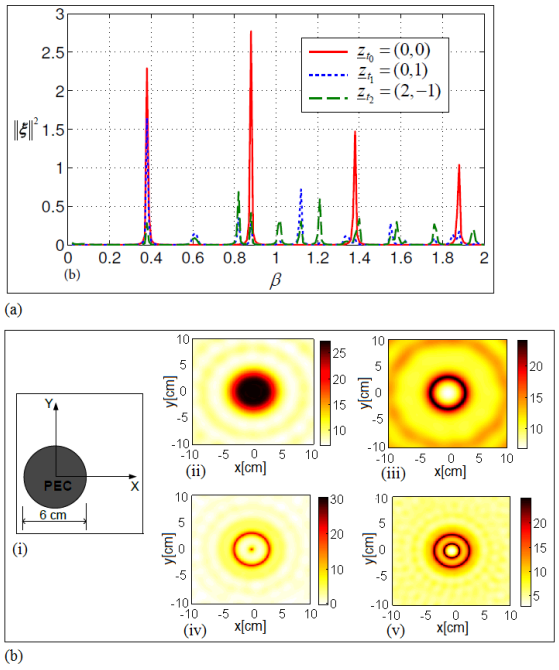

Fig. 1. The behavior of LSM for PEC: (a) LSM indicator function Magnitudes of multipoles at the sampling point $\underline{z}_{t_0}$; (b) Results of LSM for PEC: (i) Reference profile; (ii) Expected LSM results for $\beta = 0.5$; (iii) $\beta = 0.38$; (iv) $\beta = 0.61$; (iv) $\beta = 0.88$.

A. LSM on Circular PEC Objects

If the scattered fields of a circular PEC cylinder of radius a are represented with multipoles, the monopole terms of Eq. 1 are given by [5]

$$\int_0^{2\pi} \xi(\underline{z}_t, \varphi_i) d\varphi_i = \left(\frac{1}{4j}\right)\left(\frac{H_0^{(2)}(2\pi\beta)}{J_0(2\pi\beta)}\right) \quad (3)$$

Here, $\beta = \frac{a}{\lambda_b}$. λ_b is the background wavelength. The solution $\|\boldsymbol{\xi}(\underline{z}_t)\|^2$ depends on the right side of equation. The right-hand side of Eq. 3 (i.e., $\left|\frac{H_0^{(2)}(2\pi\beta)}{J_0(2\pi\beta)}\right|$) is the inverse magnitude of monopole term having the oscillatory behaviour in the range of $[1, \infty)$ with respect to β. Hence, finite values of ξ exists only for the finite values of $\left|\frac{H_0^{(2)}(2\pi\beta)}{J_0(2\pi\beta)}\right|$ (i.e., ξ is unbounded for zero-valued monopole terms). The values of $\|\boldsymbol{\xi}\|^2$are plotted in Fig. 1(a) using Eq. 1 for sample points $\underline{z}_{t_0} = (0,0), \underline{z}_{t_1} = (0,1)$ and $\underline{z}_{t_2} = (2,-1)$. It can be observed that the solution become divergent for certain values of β (eigenvalues) even-though the sample points are belong to the scatterer [8]. This behaviour is due to divergence nature of Eq. 3. More theoretical explanations can be found in [5]. The LSM reconstruction results of a PEC cylinder are shown in Fig. 1(b) for various β values. Fig. 1(b)(ii) shows the expected result obtained at $\beta = 0.5$. Fig. 1(b)(iii) through Fig. 1(b)(v) show the LSM results for β values 0.38, 0.61, and 0.88 where the eigenvalues occur.

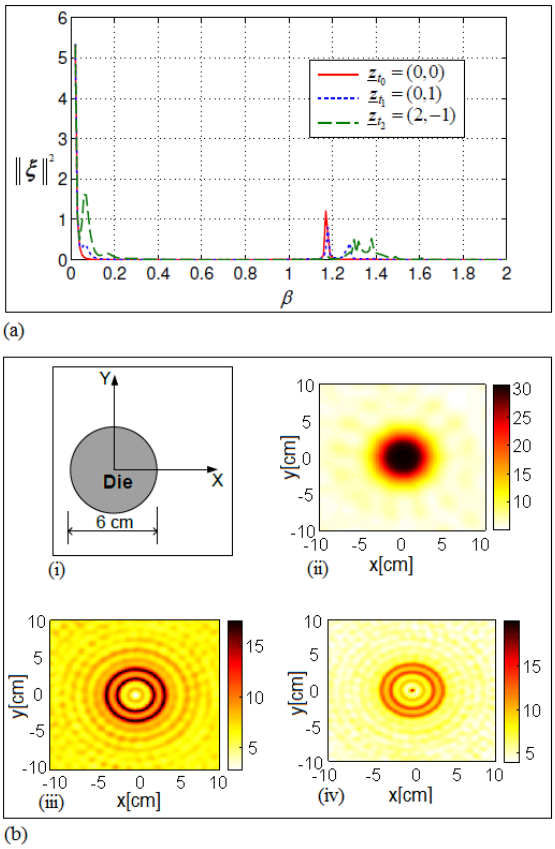

Fig. 2. The behavior of LSM for $\epsilon_r = 2$: (a) LLSM indicator function at the sampling points $\underline{z}_{t_0}$, $\underline{z}_{t_1}$ and $\underline{z}_{t_2}$. (b) Results of LSM: (i) Reference profile; (ii) Expected LSM results for $\beta = 0.5$; (iii) $\beta = 1.17$; (iv) $\beta = 1.27$.

B. LSM on Circular dielectric Objects

The LSM response for circular dielectric objects is similar to the case of PEC. Fig. 2(a) shows the indicator function for the dielectric cylinder of radius a and relative permittivity $\epsilon_r = 2$. It can be seen that less eigenvalues are found compared to the case of PEC. Number of these values gets increase for the higher values of ϵ_r [5]. The LSM reconstruction results are shown in Fig. 2(b). The expected result is seen in 2b(ii) at $\beta = 0.5$. Fig. 2b(iii) and (iv) show the effect of eigenvalues that occurs at $\beta = 1.17$ and $\beta = 1.27$.

C. LSM on Non-Circular Objects

In the previous section, the behaviour of LSM is analysed based on the nature of multipoles at the centre of circular objects. But in practical application the investigating objects are of any shape. Therefore, it is also required to investigate the performance of LSM for a non-circular objects so that the drawn conclusions remain valid in such cases. In this study, we consider a square object of length $3\sqrt{2}$ so that it can be enclosed in a circle of radius 3 (the dimension that is considered in the previous section). Here also, the values of β range from 0.02 to 2. Since it is not possible to get a closed expression for multipoles of non-circular object, we study the behaviour of the

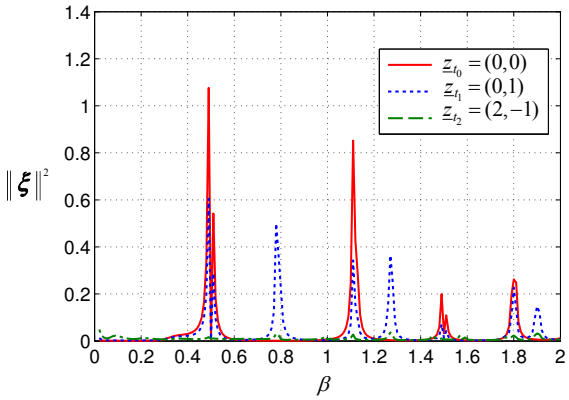

Fig. 3. The behavior of LSM for PEC square.

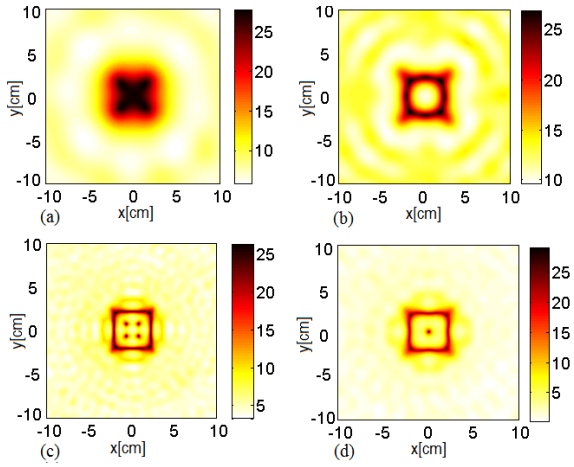

Fig. 4. LSM results for PEC square: (a) $\beta = 0.3$. (b) $\beta = 0.49$. (c) $\beta = 1.11$. (d) $\beta = 0.78$.

indicator functions only. The LSM outputs at the sampling points $\underline{z}_{t_0}$, $\underline{z}_{t_1}$, and $\underline{z}_{t_2}$ are shown in Fig. 3. By comparing the nature of plots with Fig. 1(a), it can be observed that the behavior of the indicator at $\underline{z}_{t_0}$ is similar to the case of circular object except the occurrence of eigenvalues is at larger values of β. For example in Fig. 1(a), first and second eigenvalues are located at 0.38 and 0.88, respectively whereas in the present case, these values are shifted to 0.49 and 1.11, respectively. This behaviour is not a surprise since the overall area of the square object (18 cm^2) is less compared to the area of circle (28.27 cm^2) resulting in the equivalent radius of square is 2.39. The number of multipoles to represent the scattered field increases with β (either by increase in the size or by increase in the frequency) so does the occurrence of eigenvalues. In the present case, the size of the scatterer is reduced so that these eigenvalues occur at higher values of β. A similar nature can also be seen at $\underline{z}_{t_1}$ and $\underline{z}_{t_2}$. Fig. 4 shows the results of LSM for various $\beta = 0.3$ values. It can be seen that the shape of the scatterer is estimated properly at $\beta = 0.3$ whereas the central portion is undetected at $\beta = 0.49$ and $\beta = 1.11$. These results are exactly similar to the case of circular object of Fig. 1. Unlike circular objects, the monopole terms at $\underline{z}_{t_0}$ depend on φ_i.

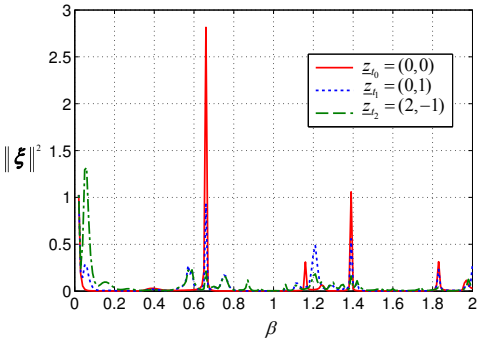

Fig. 5. The behavior of LSM for dielectric square.

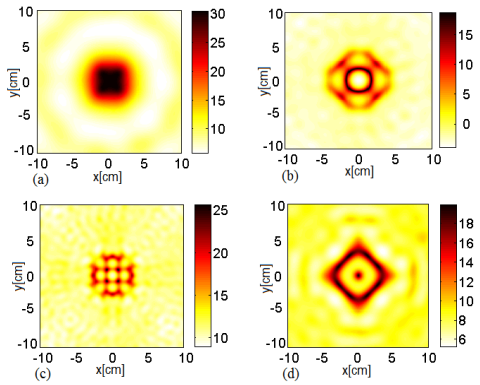

Fig. 6. LSM results for dielectric square: (a) $\beta = 0.3$, (b) $\beta = 0.66$, (c) $\beta = 1.16$, (d) $\beta = 0.57$.

Hence, one cannot say that all the monopole terms go to zero at $\beta = 0.49$. Therefore, we can only say that the effective monopole term goes to zero. Similarly, at $\beta = 0.78$, the central portion of the scatterer is detected whereas the neighbor points are undetected. It is due to the effect of higher order multipole terms [5]. For the case of dielectrics, similar results are obtained. Fig. 5 shows the indicator functions at the sampling points $\underline{z}_{t_0}$, $\underline{z}_{t_1}$, and $\underline{z}_{t_2}$ for the case of $\varepsilon_r = 4$. The results of LSM are shown in Fig. 6.

From the above discussion, it can be concluded that

- The occurrence of eigenvalues happens irrespective of the shape of the scatterer.
- The location of these eigenvalues is the function of both shape and size of the scatterer.

D. LSM on Experimental data

Here, the experimental data of two types of reference profiles are considered [9]. First, two dielectric objects of radius 1.5 cm having relative permittivity $\epsilon_r = 3$. Second, U-shaped metalic object having arm length of 8 cm and width of 0.5 cm. These objects are shown in Fig. 7 and were sequentially illuminated at 0°, 10°,...,350° with 10° incremental angular step. In each illumination, the scattered fields are measured from 60° to 300° angular span with 5° angular step with reference to the transmitter. The LSM reconstruction results of dielectric objects at 4 GHz and at 8 GHz are shown in Fig. 7(a). It can

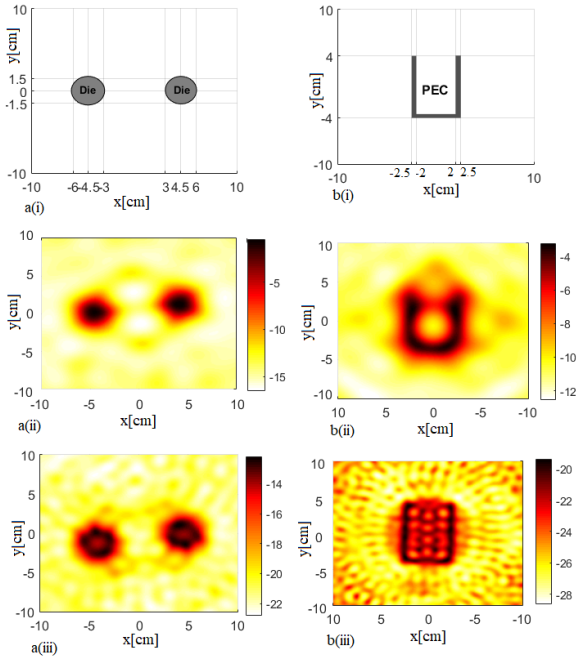

Fig. 7. LSM experimental results: (a) Two dielectric objects; (i) Reference profile, (ii) at 4 GHz, (iii) at 8 GHz. (b) U-shaped metalic object; (i) Reference profile, (ii) at 4 GHz, (iii) at 12 GHz.

be seen that smooth profile is estimated at 4 GHz whereas the central portions is partially detected at 8 GHz. It is due to the affect of eigenvalues. Similary, for PEC objects, the estimated resulst are good at 4 GHz whereas at 12 GHz, the shape is affected by the occurence of eigen values.

III. Conclusion

The behaviour of LSM for the geometric estimation of both PEC and dielectrics has been studied by representing the scattered fields with multipoles. It has been found that the LSM fails to estimates the target support for certain frequencies (eigenvalues). These values occur irrespective of the type of targets as well as the shape of targets. It has been bound that the location of these values depend on target properties.

References

[1] M. Pastorino, *Microwave imaging*. New Jersey, USA: Wiley, 2010.

[2] D. Colton, H. Haddar, and M. Piana, "The linear sampling method in inverse electromagnetic scattering theory," *Inv. Prob.*, vol. 19, no. 6, pp. S105–S137, 2003.

[3] D. Colton and P. Monk, "A linear sampling method for the detection of leukemia using microwaves," *SIAM J. Appl. Math.*, 58, pp. 926–941, 1998.

[4] D. Colton and M. Piana, "The simple method for solving the electromagnetic inverse scattering problem: the case of TE polarized waves", *Inv. Prob.*, vol. 14, no. 3, pp. 597–614, 1998.

[5] E. Mallikarjun and A. Bhattacharya, "Shape reconstruction of mixed boundary objects by linear sampling method," *IEEE Trans. Antennas Propagat.*, vol. 63, no. 7, pp. 3077–3086, 2015.

[6] M.Bertero and P. Boccacci, *Introduction to Inverse Problems in Imaging*. UK: IOP Publishing Ltd, 1998

[7] I. Catapano and L. Crocco, "An Imaging Method for Concealed Targets," *IEEE Trans. Geosci. Remote Sens.*, vol. 47, no. 5, pp. 1301–1309, 2009.

[8] J. Sun,"An eigenvalue method using multiple frequency data for inverse scattering problems," *Inv. Prob.*, vol. 28, no. 8, 025012, 2012.

[9] K. Belkebir and M. Saillard,"Special section: Testing inversion algorithms against experimental data", *Inv. Prob.*, vol. 17, pp. 1565–1571, 2001.